Realization and simulation of silicon-on-sapphire mid-infrared one-dimensional photonic crystal cavities Ⓕ⊘

Special Collection: Mid and Long Wavelength Infrared Photonics, Materials, and Devices

Yalan Si Ⓘ ; Zezhao Ju; Hui Ma; Kai Xia; Shuo Lin; Renjie Tang Ⓘ ; Boshu Sun; Chunlei Sun; Lan Li Ⓘ ; Peilong Yang ✉ Ⓘ ; Hongtao Lin ✉ Ⓘ

Check for updates

View Online

Export Citation

Articles You May Be Interested In

Dual-function optical modulation and detection in microring resonators integrated graphene/MoTe$_2$ heterojunction

Appl. Phys. Rev. (June 2024)

Mastered dispersion of material resonators: Broad corrugated waveguides working under the Littrow regime

Appl. Phys. Lett. (April 2013)

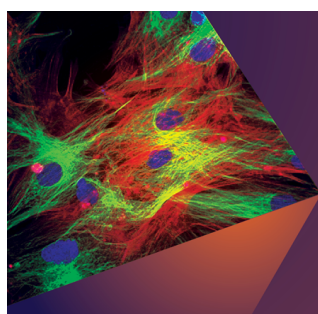Distributed feedback GaSb based laser diodes with buried grating

Appl. Phys. Lett. (April 2014)

Realization and simulation of silicon-on-sapphire mid-infrared one-dimensional photonic crystal cavities Ⓕ

View Online   Export Citation   CrossMark

Yalan Si,[1] Ⓘ Zezhao Ju,[1] Hui Ma,[1] Kai Xia,[2,3] Shuo Lin,[1] Renjie Tang,[4,5] Ⓘ Boshu Sun,[4,5] Chunlei Sun,[4,5] Lan Li,[4,5] Ⓘ Peilong Yang,[2,a] Ⓘ and Hongtao Lin[1,a] Ⓘ

AFFILIATIONS

[1]The State Key Lab of Brain-Machine Intelligence, Key Laboratory of Micro-Nano Electronics and Smart System of Zhejiang Province, College of Information Science and Electronic Engineering, Zhejiang University, Hangzhou 310027, China
[2]Laboratory of Infrared Materials and Devices, Advanced Technology Research Institute, Ningbo University, Ningbo 315211, Zhejiang, China
[3]Ningbo Institute of Oceanography, Ningbo 315832, Zhejiang, China
[4]Zhejiang Key Laboratory of 3D Micro/Nano Fabrication and Characterization, School of Engineering, Westlake University, Hangzhou, Zhejiang 310030, China
[5]Zhejiang Key Laboratory of 3D Micro/Nano Fabrication and Characterization, Westlake Institute for Optoelectronics, Fuyang, Hangzhou, Zhejiang 311421, China

Note: This paper is part of the APL Special Collection on Mid and Long Wavelength Infrared Photonics, Materials, and Devices.
[a]Authors to whom correspondence should be addressed: yangpeilong@nbu.edu.cn and honmetown@zju.edu.cn

ABSTRACT

The mid-infrared (MIR) waveband is significant for chemical and biological sensing since it covers several atmospheric windows and molecular fingerprint regions. On-chip photonic integrated one-dimensional (1D) microcavities have great potential for high-performance mid-IR sensing because of their high sensitivity and compact structure. However, high-performance 1D microcavities based on the promising silicon-on-sapphire (SoS) MIR platform have not yet been designed or realized. Based on the photonic band structure induced by 1D photonic crystals (PhC), a high-performance Bragg reflector, an inward apodized Bragg grating, and a free spectral range (FSR)-free PhC microcavity integrated system operating in the MIR waveband were developed on the SoS platform. By carefully designing the period and penetration depth of the corrugation in the Bragg reflector, a stopband of 45 nm and an extinction ratio of −12 dB were achieved. The inward apodized Bragg grating was optimized by adjusting the apodization depth and the number of periods, resulting in a quality factor of 1043 at a wavelength of 3088.4 nm. Furthermore, introducing a Fabry–Pérot (F-P) cavity between two Bragg reflectors (with side-coupled light) and precisely tuning the stopband of the Bragg reflector and the FSR of the F-P cavity enabled the realization of an FSR-free PhC microcavity. This microcavity exhibited a single deep resonance dip with subnanometer bandwidth across a record-wide operational waveband from 3025 to 3200 nm, achieving a quality factor of approximately 5090. The MIR 1D PhC microcavities on the SoS platform hold great promise for high-performance gas detection and molecular sensing in future applications.

Published under an exclusive license by AIP Publishing. https://doi.org/10.1063/5.0241260

In recent years, the mid-infrared (MIR) wavelength band (3–20 μm) contains multiple atmospheric windows,[1,2] which has natural advantages in sensing, thermal imaging, and free-space optical communication.[3] Furthermore, MIR integrated photonic devices continue to play an important role in industrial detection, scientific research, medical diagnosis, and civilian life, since integrated photonics provides unparalleled advantages in terms of size, weight, and power (SWaP) consumption, in addition to enhanced robustness, compared with systems that are assembled from discrete components.[4] With the advancement of micro and nanofabrication technology and further exploration of materials science,[5,6] a series of high-performance on-chip integrated passive devices, such as waveguides,[7–12] grating

27 August 2025 06:52:29

couplers,[13–15] directional couplers,[16,17] micro-ring resonators,[18–20] photonic crystal cavities,[21] and inverse design devices,[22,23] have been designed and realized in MIR waveband.

Among these devices, 1D PhC microcavities in the MIR range have attracted significant attention for their high integration density, exceptional sensitivity, and design flexibility.[3] Over the recent decades of research, the realm of 1D PhC microcavities have witnessed remarkable progress, evincing unparalleled performance capabilities at wavelengths below 3 μm.[24–26] Nevertheless, research on MIR remains limited and hindered by challenges posed by immature photonic platforms, intricate manufacturing methodologies, and constrained availability of suitable light sources. Notably, there are instances of 1D PhC microcavity operating above 3 μm that have been realized on the basis of the chalcogenide glass platform.[27,28] Silicon-on-sapphire (SoS) is an important material platform for mid-infrared integrated photonics, because it has a wide transparent window up to 5.5 μm, high refractive index contrast ($\Delta n = 1.96$) between the core and the sapphire, and CMOS compatibility.[3,29] Based on the SoS photonic platform, many high-performance MIR passive photonic devices, such as waveguides,[30] ring resonators,[31] and photonic crystal waveguides,[32] have been demonstrated and realized on the SoS platform. However, high-performance 1D PhC microcavities based on the promising SoS platform have yet to be designed and demonstrated.

In this work, we realized two distinct high-performance 1D PhC microcavities: inward apodized Bragg grating and free spectral range (FSR)-free photonic crystal microcavity on the SoS platform, leveraging the unique properties of Bragg reflectors as the foundational element. This achievement marks a significant advancement in photonic integration and microcavity technology. First, outstanding-performance Bragg reflectors were designed and fabricated, achieving a stopband width of 45 nm and an extinction ratio of -12 dB through meticulous optimization of the corrugation width and period. Building on this foundation, a superior inward apodized Bragg grating was developed by modulating the corrugation width to follow a parabolic profile, resulting in a quality factor of 1043 at a wavelength of 3084.4 nm. Finally, by integrating an F-P cavity, Bragg reflectors, and a bent waveguide, we have achieved an FSR-free PhC microcavity design. By fine-tuning the F-P cavity and the stopband of the Bragg reflectors, we realized an FSR-free response spanning over a hundred nanometers, while attaining a remarkable quality factor of 5090 at a wavelength of 3054 nm. The devices we have realized hold great potential for applications in optical communications and sensing.

We proposed a device structure concept for gas detection that can be used to detect gases such as HCN and CH$_4$. As shown in Fig. 1(a), the design first cascades two Bragg reflectors to filter the broadband input light source. Next, the inward apodized Bragg grating is used to identify the type of gas by detecting shifts in its resonant wavelength. Finally, thermal tuning of the FSR-free photonic crystal microcavity filters out different resonant wavelengths of the inward apodized Bragg grating, enabling the calculation of gas concentration through spectral intensity changes detected by the detector. The Bragg reflector serves as the foundation of this design. Figure 2(a) illustrates the schematic of a Bragg reflector in a strip waveguide using rectangular sidewall corrugations. The corrugation width on each sidewall is Δw, the waveguide width is W, the number of periods in the Bragg reflector is N, and the period is Λ. The Bragg reflector features periodic variations in refractive index along the direction of optical mode propagation, as depicted in Fig. 2(a). At each boundary, the transmitted light undergoes reflection, and the relative phase of the reflected signal is determined by the grating period and the wavelength. The repeated modulation of the effective refractive index results in multiple distributed reflections. The Bragg wavelength is given by

$$\lambda_B = 2\Lambda n_{eff}, \tag{1}$$

where Λ represents the grating period and n_{eff} denotes the effective refractive index of the grating structure.

The peak power reflectivity at the Bragg wavelength is given by

$$R_{peak} = \tanh^2(\kappa L). \tag{2}$$

The coupling coefficient is $\kappa = \pi\Delta n/(2\lambda_B)$, and $\Delta n = n_{eff1} - n_{eff2}$.
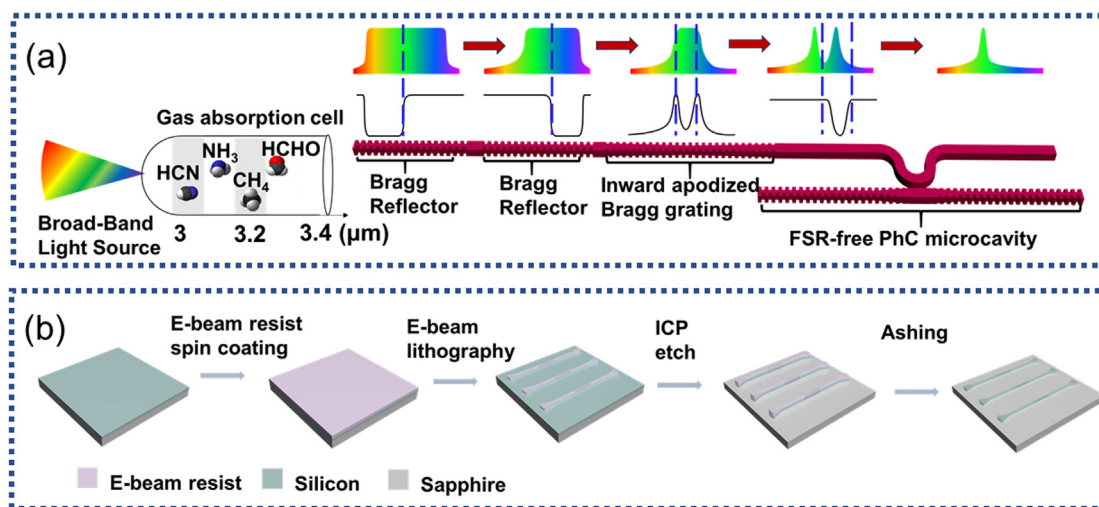
FIG. 1. (a) Schematic diagram of cascade device. (b) Schematic of the fabrication process.
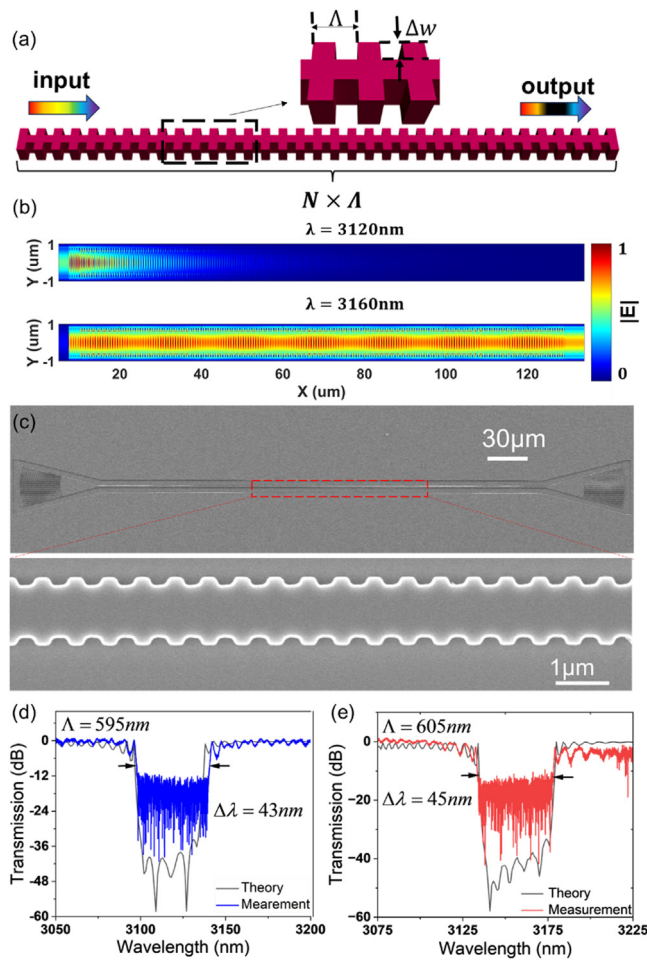
FIG. 2. Simulation and characterization of Bragg reflectors. (a) Schematic diagram of the Bragg reflector structure. (b) Normalized simulated field intensity distribution of |E| at the wavelengths of 3120 and 3160 nm. (c) SEM image of the fabricated Bragg reflector device. (d) Simulated and measured transmission spectra of the Bragg reflector with the period of 595 nm. (e) Simulated and measured transmission spectra of the Bragg reflector with the period of 605 nm.

The bandwidth between the first nulls surrounding the main reflection peak can be determined by

$$\Delta\lambda = \frac{\lambda_B^2}{\pi n_g}\sqrt{\kappa^2 + \left(\frac{\pi}{L}\right)^2}. \quad (3)$$

κ is typically defined as the coupling coefficient of the grating, which can be interpreted as the amount of reflection per unit length. n_g denotes the group refractive index of the structure and L represents the length of the grating.

In this work, all of our device simulations were completed using FDTD simulation. After determining the device parameters, we fabricated the device based on the fabrication process shown in Fig. 1(b). After spin-coating the wafer with photoresist (ARP 6200.13), lithography was performed via electron beam lithography (Raith Voyager). Then, the silicon was then etched to a depth of 600 nm via inductively

coupled plasma (ICP) etching. Finally, the residual resist was removed via a piranha solution. Characterization of the fabricated devices was performed using a vertical fiber coupling test system. The devices were illuminated by the supercontinuum laser (manufactured in the Laboratory of Infrared Materials and Devices at Ningbo University) through the vertical fiber, and the transmission spectra of our device were measured via a spectrometer (YOKOGAWA AQ6377).

Figure 2(a) illustrates the schematic structure of the Bragg reflector. The waveguide width of the Bragg reflector calculated by using the FDE (finite difference eigenmode) simulation is $1.2\,\mu m$ to ensure single-mode transmission. Given that the designed Bragg reflector will subsequently be integrated as a reflector in the FSR-free PhC microcavity, and based on the principles of the FSR-free PhC microcavity, we require the Bragg reflector to possess a narrow stopband and high reflectivity. According to Eq. (2), an increase in corrugation width directly correlates with an expansion of the stopband. Therefore, the designed corrugation width must be modest. Additionally, considering the limitations of the fabrication process, we have designed a corrugation width of 150 nm. Then, we can calculate the period of the Bragg reflector operating at $3.1\,\mu m$ to be 595 nm by using Eq. (1). Based on Eqs. (2) and (3), augmenting the number of periods enhances both the peak reflectivity and the stopband width of Bragg reflector. Consequently, to meet the stipulated requirements, the device is configured with 200 periods, and the extinction ratio of the simulation results obtained of the device reaches $-42\,dB$. The normalized field electric intensity distribution of |E| in the stopband (3120 nm) and passband (3160 nm) is illustrated in Fig. 2(b). The field intensity distribution indicates that within the stopband wavelength range, the light is almost entirely reflected, whereas light outside the stopband is transmitted with nearly no reflection. Figure 2(c) shows the scanning electron microscope (SEM) image of the fabricated device. The measured transmission spectra illustrated in Fig. 2(d) closely match the simulated result, with an extinction ratio of $-12\,dB$ (the inaccuracies in the measurement process led to lower extinction ratio measurement results). Furthermore, a Bragg reflector with the period of 605 nm is also verified, as shown in Fig. 2(e), which exhibits 43 nm stopband centered at a wavelength of 3158 nm. By combining two Bragg reflectors with distinct periods, we observed that an increase of 10 nm in the period results in a shift of approximately 35 nm in the Bragg wavelength. Leveraging this finding, we can precisely tune the operating wavelength of the Bragg wavelength by adjusting the period, thereby facilitating the subsequent design of FSR-free devices.

We designed and implemented an inward apodized Bragg grating by cascading Bragg gratings (with an inward grating profile apodized by a quadratic function[33,34]) as the cavity and two Bragg reflectors as the mirrors, as illustrated in Fig. 3(a). Taking the fabrication complexity and the operating wavelength of the device into consideration, the deepest and shallowest corrugation width is, respectively, set as $w_d = 250$ nm, $w_s = 150$ nm, and the period and number of periods of the Bragg reflector are, respectively, set as $\Lambda = 596$ nm and $N_r = 10$. When the period number N is 100, the simulated normalized field intensity distribution |E| for the resonant wavelength (3087.7 nm) and non-resonant wavelength (3076 nm) are shown in Fig. 3(b), while the simulated transmission spectra are shown in Fig. 3(d). Additionally, the SEM image of the fabricated device is illustrated in Fig. 3(c) with a quality factor reaching 1043 at the wavelength of 3088.4 nm as presented in Fig. 3(e).
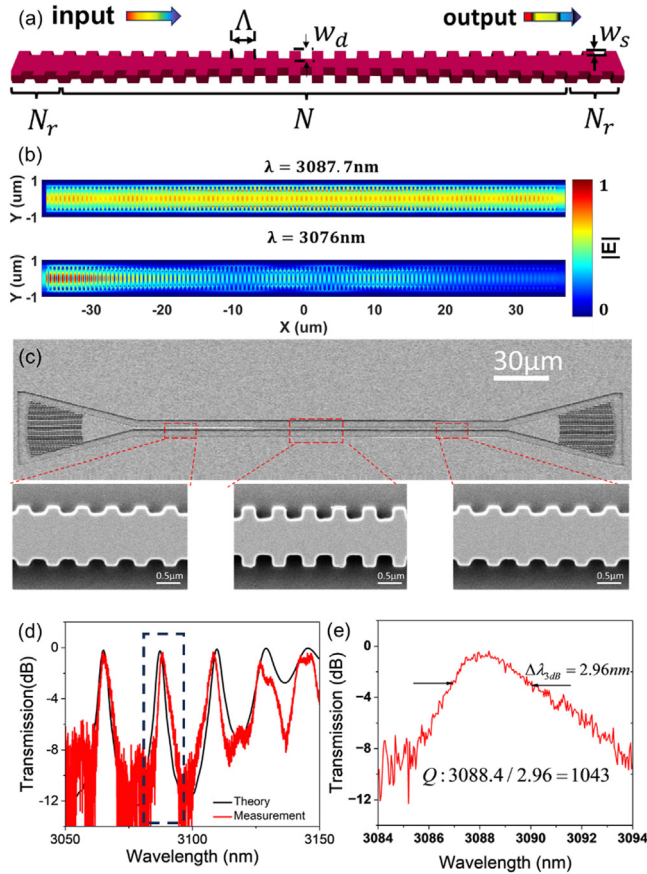
FIG. 3. Simulation and characterization of an inward apodized Bragg grating. (a) Structural diagram of the inward apodized Bragg grating. (b) Normalized simulated field intensity distribution of $|E|$ at the wavelengths of 3087.7 and 3076 nm. (c) SEM image of the fabricated inward apodized Bragg grating device with $N = 100$. (d) Transmission spectra of the simulated device and the measured device. (e) Transmission spectra of resonant wavelength (3087.7 nm).

FIG. 4. Simulation and characterization of FSR-free PhC microcavities. (a) Schematic diagram of the FSR-free PhC microcavity structure. (b) Simulated electric field distribution at wavelengths of 3054 and 3120 nm for the device with a period of 580 nm. (c) SEM image of the FSR-free PhC microcavity. (d) Simulated and measured transmission spectra for devices with periods of 580, 590, 600, 610, and 620 nm. (e) Transmission spectra of fabricated devices with periods of 580 nm.

Based on the above-mentioned high-performance Bragg reflectors, we designed an F-P cavity and ultimately realized an FSR-free PhC microcavity through side coupling,[25] as shown in Fig. 4(a). The F-P cavity is formed when a central single-mode waveguide is flanked by two Bragg reflectors acting as side-reflecting mirrors. A single-mode waveguide connects two lateral Bragg reflectors, with a taper/grating introduced between them to reduce scattering losses at the cavity–mirror interface. The key parameters of the device include the length of the central waveguide ($Lc = 1.5\,\mu m$), the bending radius ($R = 60\,\mu m$), the coupling gap ($G = 100\,nm$), and the corrugation width ($\Delta w = 150\,nm$). The resonant spectra of the device are determined by the stopband width $\Delta\lambda_{sb}$ of the Bragg reflector and the FSR of the F-P cavity. When $\Delta\lambda_{sb} < FSR_{FP}$, only a single resonant mode within the stopband of the Bragg reflector is excited and enhanced in the F-P cavity, which appears as a dip in the transmission spectra. If the F-P cavity has a narrow bandwidth, none of the resonant modes overlap with the stopband, resulting in no dip being observed in the transmission spectra. Figure 4(d) shows the simulated transmission spectra of 1D PhC microcavity with different periods. At the resonant
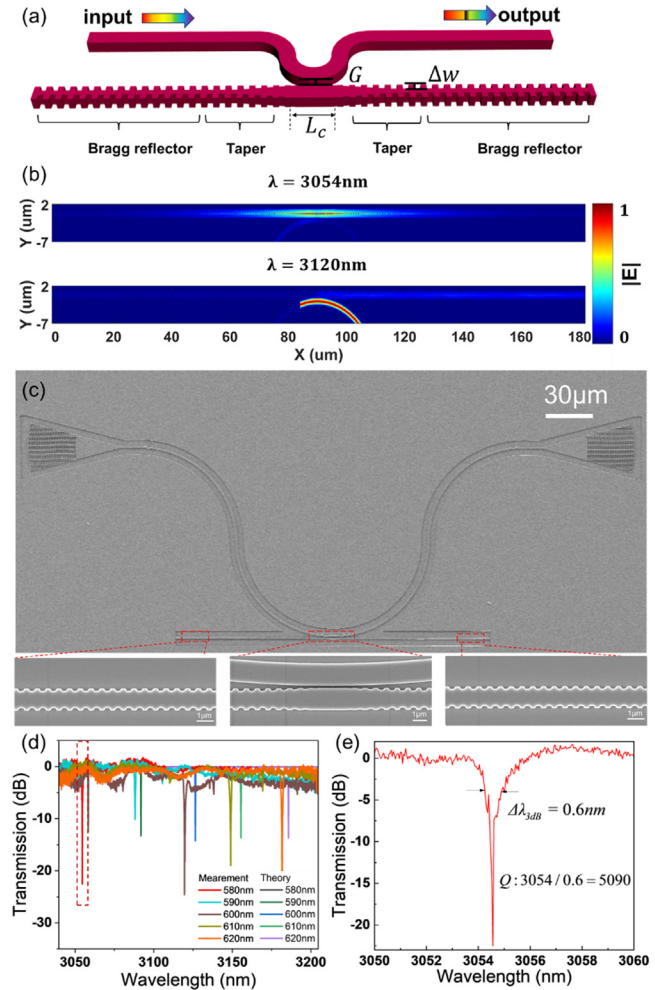
wavelength (3054 nm), as shown in Fig. 4(b), light is trapped in the cavity. We then compared the simulation results with experimental results [the SEM image is shown in Fig. 4(c)]. For the device with a period of 580 nm, a significant resonant phenomenon is observed at 3054 nm, with an extinction ratio of $-22\,dB$, as shown in Fig. 4(d). At this point, the full width at half maximum (FWHM) is 0.6 nm, and the quality factor reaches 5090 as shown in Fig. 4(e). As shown in the table, the device we prepared has relatively superior performance. Due to the limitation of the resolution of the spectrometer, devices with high Q values are difficult to measure. However, we can design devices with better Q values by optimizing the design. Table I summarizes research of the past decade on passive photonic crystal devices in the mid-infrared range. As shown in the table, the quality factor (Q value) of the photonic crystal devices we fabricated demonstrates comparable

TABLE I. Passive mid-IR photonic crystals and their state-of-the-art performance.

Material platform	Wavelength	Geometry	Q	Type of resonance
Suspended Si[21]	4.38–4.42 μm	2D phc	13 600 (Experiment)	Peak
SoS[32]	3.43 μm	2D phc	3500 (Experiment)	Peak
$Ge_{23}Sb_7S_{70}$ ChG on CaF_2[27]	5.2 μm	1D phc	2000 (Experiment)	Peak
Germanium[35]	2.5 μm	2D phc	200 (Experiment)	Peak
Silicon[36]	3.73 μm	2D phc	3.4×10^4 (Simulation)	Peak
Silicon[37]	4.93 μm	2D phc	873 (Simulation)	Peak
SoS (this work)	3.054 μm	1D phc	5090 (Experiment)	Dip

performance. At the same time, we can see that we have realized one-dimensional photonic crystal device with a dip-type resonance in the MIR band. However, due to limitations in experimental equipment, particularly the resolution of the spectrometer, the Q values measured in our experiments cannot reach the theoretical optimum. Nevertheless, through optimization of the device design, we can use simulation techniques to predict and achieve even higher Q values, which opens up possibilities for further research and improvements in device performance.

In summary, we innovatively proposed a gas detection device structure that works in the mid-infrared band and realized the basic device of this detection structure. At the same time, the devices prepared: Bragg reflectors, inward apodized Bragg grating, and FSR-free PhC microcavity based on the SoS platform and working in the mid-infrared band are proposed. The fabricated Bragg reflectors exhibit a stopband of approximately 45 nm with an extinction ratio of approximately −12 dB. By utilizing the designed Bragg reflectors and the FSR configuration of the F-P cavity, we realized an FSR-free PhC microcavity that achieved a single deep resonance dip within the wavelength range of 3025–3200 nm, and the quality factor reaches 5090 at the wavelength of 3054 nm. Additionally, we have developed an inward apodized Bragg grating operating at 3088.4 nm with a quality factor of 1043. The MIR 1D PhC microcavities are compatible with various photonic integration platforms, and we anticipate that these devices will demonstrate significant application potential in the field of MIR detection and sensing.

AUTHOR DECLARATIONS
Conflict of Interest

The authors have no conflicts to disclose.

Author Contributions

Yalan Si: Data curation (lead); Investigation (lead); Methodology (equal); Writing – original draft (lead). **Zezhao Ju:** Software (supporting); Validation (lead); Writing – original draft (supporting). **Hui Ma:** Methodology (equal); Writing – original draft (supporting). **Kai Xia:** Validation (supporting). **Shuo Lin:** Software (supporting). **Renjie Tang:** Software (supporting); Writing – review & editing (supporting). **Boshu Sun:** Writing – review & editing (supporting). **Chunlei Sun:** Software (supporting); Writing – review & editing (supporting). **Lan Li:** Writing – review & editing (supporting). **Peilong Yang:** Funding acquisition (equal). **Hongtao Lin:** Conceptualization (equal); Funding acquisition (equal); Supervision (equal); Writing – review & editing (equal).

DATA AVAILABILITY

The data that support the findings of this study are available from the corresponding authors upon reasonable request.

REFERENCES

[1]D. Pile, N. Horiuchi, R. Won, and O. Graydon, Nat. Photonics **6**(7), 407 (2012).
[2]L. Tong, X. Huang, P. Wang, L. Ye, M. Peng, L. An, Q. Sun, Y. Zhang, G. Yang, Z. Li, F. Zhong, F. Wang, Y. Wang, M. Motlag, W. Wu, G. J. Cheng, and W. Hu, Nat. Commun. **11**(1), 2308 (2020).
[3]R. Soref, Nat. Photonics **4**(8), 495 (2010).
[4]H. Lin, Z. Luo, T. Gu, L. C. Kimerling, K. Wada, A. Agarwal, and J. Hu, Nanophotonics **7**(2), 393 (2017).
[5]A. J. Hoffman, L. Alekseyev, S. S. Howard, K. J. Franz, D. Wasserman, V. A. Podolskiy, E. E. Narimanov, D. L. Sivco, and C. Gmachl, Nat. Mater. **6**(12), 946 (2007).
[6]S. Assali, S. Koelling, Z. Abboud, J. Nicolas, A. Attiaoui, and O. Moutanabbir, J. Appl. Phys. **132**(17), 175304 (2022).
[7]G. Z. Mashanovich, M. M. Milošević, M. Nedeljkovic, N. Owens, B. Xiong, E. J. Teo, and Y. Hu, Opt. Express **19**(8), 7112 (2011).
[8]S. Khan, J. Chiles, J. Ma, and S. Fathpour, Appl. Phys. Lett. **102**(12), 121104 (2013).
[9]V. Singh, P. T. Lin, N. Patel, H. Lin, L. Li, Y. Zou, F. Deng, C. Ni, J. Hu, J. Giammarco, A. P. Soliani, B. Zdyrko, I. Luzinov, S. Novak, J. Novak, P. Wachtel, S. Danto, J. D. Musgraves, K. Richardson, L. C. Kimerling, and A. M. Agarwal, Sci. Technol. Adv. Mater. **15**(1), 014603 (2014).
[10]M. Nedeljkovic, J. S. Penadés, C. J. Mitchell, A. Z. Khokhar, S. Stanković, T. D. Bucio, C. G. Littlejohns, F. Y. Gardes, and G. Z. Mashanovich, IEEE Photonics Technol. Lett. **27**(10), 1040 (2015).
[11]B. Kuyken, T. Ideguchi, S. Holzner, M. Yan, T. W. Hänsch, J. Van Campenhout, P. Verheyen, S. Coen, F. Leo, R. Baets, G. Roelkens, and N. Picqué, Nat. Commun. **6**(1), 6310 (2015).
[12]B. Dong, X. Guo, C. P. Ho, B. Li, H. Wang, C. Lee, X. Luo, and G. Q. Lo, IEEE Photonics J. **9**(3), 4501410 (2017).

[13]N. Chen, B. Dong, X. Luo, H. Wang, N. Singh, G.-Q. Lo, and C. Lee, Opt. Express **26**(20), 26242 (2018).

[14]Y. Liu, L. Xia, T. Li, Y. Sun, P. Zhou, L. Shen, and Y. Zou, Opt. Lett. **48**(2), 239 (2023).

[15]Y. Hu, W. He, Y. Sun, Q. Yi, S. Xing, Z. Yan, L. Xia, T. Li, P. Zhou, J. Zhang, L. Shen, and Y. Zou, Opt. Express **31**(23), 39079 (2023).

[16]B. Dong, T. Hu, X. Luo, Y. Chang, X. Guo, H. Wang, D.-L. Kwong, G.-Q. Lo, and C. Lee, Nanomaterials **8**(11), 893 (2018).

[17]A. Thottoli, G. Biagi, A. S. Vorobev, M. Giglio, G. Magno, L. O'Faolain, and M. Grande, Sci. Rep. **13**(1), 22720 (2023).

[18]Y. Xia, C. Qiu, X. Zhang, W. Gao, J. Shu, and Q. Xu, Opt. Lett. **38**(7), 1122 (2013).

[19]R. Armand, M. Perestjuk, A. D. Torre, M. Sinobad, A. Mitchell, A. Boes, J.-M. Hartmann, J.-M. Fedeli, V. Reboud, P. Brianceau, A. De Rossi, S. Combrié, C. Monat, and C. Grillet, APL Photonics **8**(7), 071301 (2023).

[20]R. Guo, Q. Lang, Z. Zhang, H. Hu, T. Liu, J. Wang, and Z. Cheng, Chip **3**(3), 100104 (2024).

[21]R. Shankar, R. Leijssen, I. Bulu, and M. Lončar, Opt. Express **19**(6), 5579 (2011).

[22]J. Xu, Y. Liu, X. Guo, Q. Song, and K. Xu, Opt. Express **30**(15), 26266 (2022).

[23]X. Lin, M. Wei, K. Lei, S. Yang, H. Ma, C. Zhong, Y. Luo, D. Li, J. Li, C. Lin, W. Zhang, S. Dai, X. Hu, L. Li, E. Li, and H. Lin, Laser Photonics Rev. **17**(2), 2200445 (2023).

[24]H. Lin, Y. Song, Y. Huang, D. Kita, S. Deckoff-Jones, K. Wang, L. Li, J. Li, H. Zheng, Z. Luo, H. Wang, S. Novak, A. Yadav, C.-C. Huang, R.-J. Shiue, D. Englund, T. Gu, D. Hewak, K. Richardson, J. Kong, and J. Hu, Nat. Photonics **11**(12), 798 (2017).

[25]C. Sun, C. Zhong, M. Wei, H. Ma, Y. Luo, Z. Chen, R. Tang, J. Jian, H. Lin, and L. Li, Photonics Res. **9**(6), 1013 (2021).

[26]M. H. Haron, B. Y. Majlis, and A. R. Zain, Photonics **8**(4), 99 (2021).

[27]H. Lin, L. Li, F. Deng, C. Ni, S. Danto, J. D. Musgraves, K. Richardson, and J. Hu, Opt. Lett. **38**(15), 2779 (2013).

[28]D. Conteduca, F. Dell'Olio, C. Ciminelli, and M. N. Armenise, Appl. Opt. **54**(9), 2208 (2015).

[29]R. A. Soref, S. J. Emelett, and W. R. Buchwald, J. Opt. A: Pure Appl. Opt. **8**(10), 840 (2006).

[30]T. Baehr-Jones, A. Spott, R. Ilic, A. Spott, B. Penkov, W. Asher, and M. Hochberg, Opt. Express **18**(12), 12127 (2010).

[31]A. Spott, Y. Liu, T. Baehr-Jones, R. Ilic, and M. Hochberg, Appl. Phys. Lett. **97**(21), 213501 (2010).

[32]Y. Zou, S. Chakravarty, and R. T. Chen, Appl. Phys. Lett. **107**(8), 081109 (2015).

[33]Q. Quan and M. Loncar, Opt. Express **19**(19), 18529 (2011).

[34]Q. Quan, P. B. Deotare, and M. Loncar, Appl. Phys. Lett. **96**(20), 203102 (2010).

[35]T.-H. Xiao, Z. Zhao, W. Zhou, M. Takenaka, H. K. Tsang, Z. Cheng, and K. Goda, Opt. Lett. **42**(15), 2882 (2017).

[36]L. Kassa-Baghdouche and E. Cassan, Opt. Quantum Electron. **52**(5), 260 (2020).

[37]T. X. Hoang, H.-S. Chu, F. J. García-Vidal, and C. E. Png, J. Opt. **24**(9), 094006 (2022).

27 August 2025 06:52:29